Article

Not peer-reviewed version

A Composite Tool for Forecasting El-Nino. The Case of the 2023–2024 Event

Costas Varotsos *, Nicholas V. Sarlis, Yuri Mazei, Damir Saldaev, Maria Efstathiou

Posted Date: 5 February 2024

doi: 10.20944/preprints202402.0202.v1

Keywords: El Niño; non-linear dynamics; natural time analysis; symmetry breaking; receiver operating characteristics; nowcasting; extreme events; entropy

 doi:10.20944/preprints202402.0202.v1

Article

A Composite Tool for Forecasting El-Niño. The Case of the 2023–2024 Event

Costas Varotsos [1,2,*], Nicholas V. Sarlis [3], Yuri Mazei [1,4,5], Damir Saldaev [1,4] and Maria Efstathiou [2]

[1] Department of Biology, Shenzhen MSU-BIT University, Shenzhen, 518172, China; covar@phys.uoa.gr
[2] Department of Environmental Physics and Meteorology, National and Kapodistrian University of Athens, Zografos, 15784, Greece; mefstathiou2014@gmail.com
[3] Section of Condensed Matter Physics, Department of Physics, National and Kapodistrian University of Athens, Zografos, 15784, Greece; nsarlis@phys.uoa.gr
[4] Department of General Ecology and Hydrobiology, Lomonosov Moscow State University, Leninskiye Gory, 1, Moscow, 119991, Russia; k-brom@yandex.ru
[5] Severtsov Institute of Ecology and Evolution, Russian Academy of Sciences, Leninskiy Ave. 33, Moscow, 117071, Russia; yurimazei@mail.ru
* Correspondence: covar@phys.uoa.gr

Abstract: Remotely sensed data play a crucial role in monitoring the El-Niño/La-Niña Southern Oscillation (ENSO), which is an oceanic-atmospheric phenomenon occurring quasi-periodically with several impacts worldwide, such as specific biological and global climate responses. Since 1980, Earth has witnessed three strong ENSO events (1982–1983, This study aims, 2015-2016). In September 2022, La-Niña entered its third year and was unlikely to continue through 2023. Instead, since 2022 forecasts pointed to a transition from La-Nina to a Neutral phase in summer or late 2023. The onset of the El-Niño occurred around April 2023, and it is anticipated by sophisticated models to be a strong event through the Northern Hemisphere winter (December 2023 - February 2024). The aim of this study is to demonstrate the ability of the combination of two new methods to improve the accuracy of the above claim because El-Niño apart from climate anomalies, significantly impacts Earth's ecosystems and human societies, regulating the spread of diseases by insects (e.g., malaria and dengue fever), and influencing nutrients, phytoplankton biomass, and primary productivity. This is done by exploring first the previous major El-Niño events in the period January 1876-July 2023. Our calculations show that the ongoing 2023-2024 El-Niño will not be the strongest.

Keywords: El Niño; non-linear dynamics; natural time analysis; symmetry breaking; receiver operating characteristics; nowcasting; extreme events; entropy

1. Introduction

Walker and Bliss [1] observed that when Tahiti's air pressure at sea level was stronger than average, Darwin's was weaker, and vice versa. After several decades this "Southern Oscillation" (SO) was also linked to a known phenomenon since the 19th century of warmer than average ocean water off the Pacific coast of South America (Peru-Ecuador). This peaks annually around Christmas and is therefore called El Niño (the little boy - the birth of Christ), a name dating to the 1800s. However, this term has been used in more recent years for the enhanced warmings that occur every 3-7 years (measured by the sea surface temperature -SST- along the Peru-Ecuador coast) [2]. The opposite condition is called La Niña [3].

The coupling of these two phenomena provides the pattern of the El Niño–Southern Oscillation (ENSO) [4]). Although ENSO originates in the tropical Pacific Ocean, its climatic effects are felt worldwide (e.g., from droughts in Indonesia and Australia to storms and floods in Ecuador and the USA) due to the changes it causes in global atmospheric circulation patterns. For this ENSO is the strongest source of natural variability in the Earth's climate system [5]. Traditionally a measure of the large-scale variations in atmospheric pressure between the western and eastern tropical Pacific

 doi:10.20944/preprints202402.0202.v1

(between Tahiti and Darwin, Australia) is the Southern Oscillation Index (SOI) which indicates the state of the SO, particularly during episodes of El Niño and La Niña [6].

These enhanced interactions between the ocean and atmosphere result in important consequences for people and ecosystems across the globe, with sometimes catastrophic effects on the ecological system [7,8]. These extreme events can produce secondary effects that affect food supplies and prices, heatwaves, forest and brush fires, and other severe hydrometeorological events, creating additional economic and political consequences (e.g., famines and political strife) [9,10]. The biological consequences of an El Niño event also include sudden population growth or decline that can lead to population genetic problems and adaptability to future environmental changes [11]. Also included is the out-break of epidemics of diseases transmitted by insects, due to the decrease in rainfall and the increase in temperature in various regions of the world (e.g., Colombia) which cause high mosquito breeding rates [12].

While we mostly understand how ENSO works and its effects around the world, we still don't know how ENSO will change as the planet warms and what its effect on global weather and climate will then be [13]. For example, we know that El Niño is a source of anomalous ocean conditions that lead to specific biological responses that regulate nutrients, and phytoplankton biomass, impacting marine life and primary productivity [14.] Effects on higher organisms such as fish, seabirds, and marine mammals are also suggested, but several years of additional observations are required to determine them precisely [15]. In this regard, coral records and other proxies suggest that ENSO has been happening for thousands of years. Studies as well as the most recent Intergovernmental Panel on Climate Change report conclude that there is no agreement among climate models on how ENSO will be affected by climate change [16].

One way to detect the arrival of El Niño is to analyse satellite and ocean measurements of SST. After three consecutive La Niña years, the spring of 2023 saw the return of El Niño according to data from the Sentinel-6 Michael Freilich and Sentinel-3B satellites (Fig. 1). The Sentinel-6 Michael Freilich satellite is designed to measure ocean height, while Sentinel-3 is designed to measure sea surface topography, sea and land surface temperature, and colour [17].

Because in its presence warmer water expands to fill more volume, while colder water contracts, ocean warming causes a rise in sea surface height that can be detected by satellite measurements and thus signal the occurrence of El Niño. A commonly used measure of ENSO strength is the mean SST anomaly (or the Oceanic Niño Index-ONI, i.e., the variations of the three-month running average of SST) in the Niño-3.4 region of the equatorial Pacific, a box extending from 170°E–120°E and 5°S–5°N (Fig. 1-top). According to the latest estimates (of 14 Dec. 2023) (Figure 1-bottom), El Niño will continue during the Northern Hemisphere winter, while the transition to a neutral ENSO state is favoured in April-June 2024 (with 60% probability).

The condition for the presence of El Niño is for this anomaly to equal or exceed 0.5 °C persisting for several months. Glantz and Ramirez [10] suggested that the value of 0.7 °C identifies a tipping point where the El Niño event is locked in, providing sufficient time for societal decision-makers to take mitigation measures. When the anomaly exceeds 1.0 °C then it is considered that the El Niño is of moderate strength while 1.5 °C is the threshold for a strong event.

The climate models attempt to predict the features of the upcoming ENSO events to provide in time the necessary reliable information to the population to get safety measures well in advance [18]. However, the predictions provided by the models are sometimes not accurate enough because the ocean-atmosphere system is complex and complicated. For example, in 29-Sept-2015 the Australian Government Bureau of Meteorology (BOM) reported that "The 2015 El Niño could be the strongest El Niño since 1997–98" and that the 2015-2016 El Niño event "was likely to peak towards the end of 2015" (http://www.bom.gov. au/climate/enso/archive/ensowrap_20150929.pdf). Similar information was also reported on 8- Oct- 2015 by the Climate Prediction Center, National Centers for Environmental Prediction, NOAA / National Weather Service (http://www.cpc.ncep.noaa.gov/products/analysis_monitoring/enso_disc_oct2015/ensodisc.pdf).

 doi:10.20944/preprints202402.0202.v1

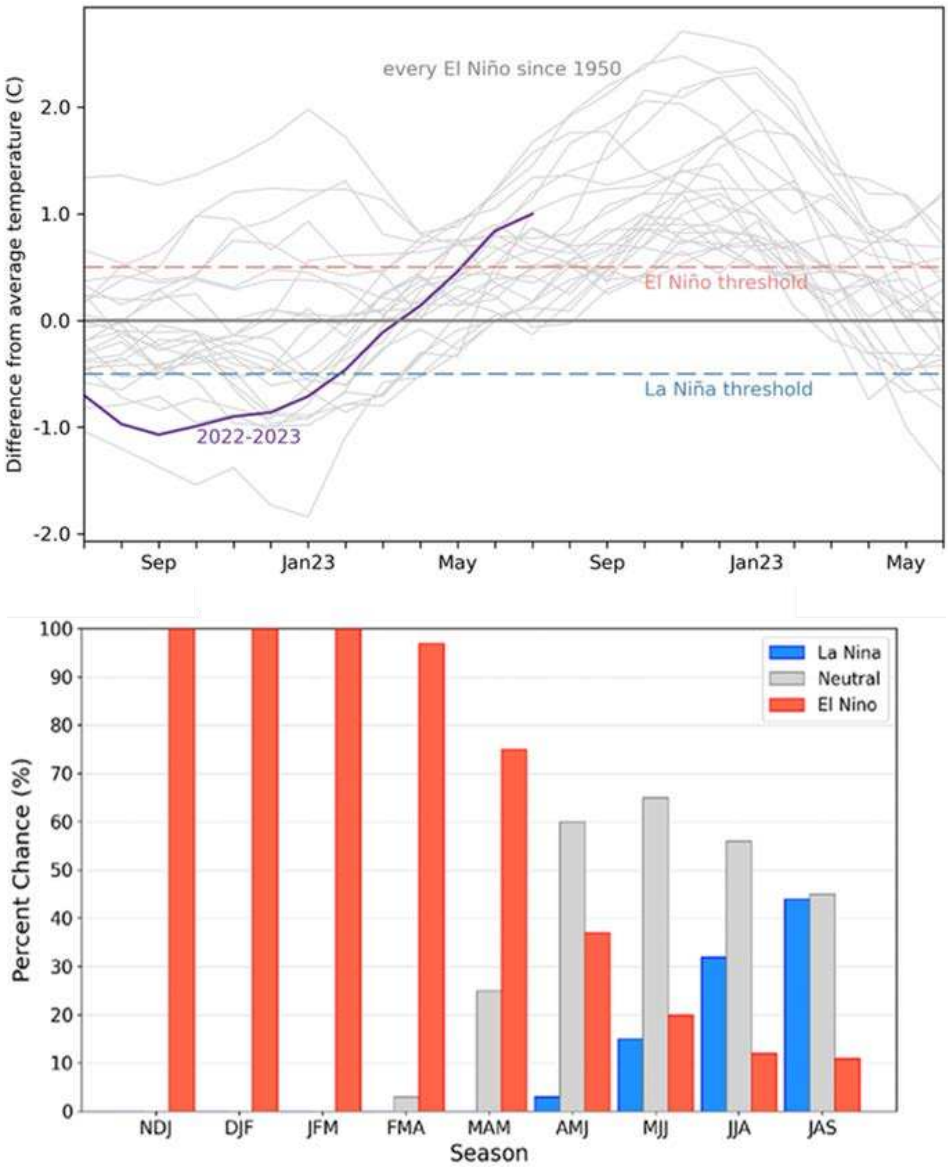

Figure 1. (Top): Two-year history of sea surface temperatures in the Niño-3.4 (the temperature anomaly of the surface of the central tropical Pacific Ocean currently defined as the departure from the 1991–2020 average) for all events evolving into El Niño since 1950 (gray lines) and the current event (purple line). (Bottom): Official ENSO probabilities for the Niño-3.4 SST index (5°N-5°S, 120°W-170°W), updated 14 December 2023 (Credit: NOAA climate.gov). (https://www.cpc.ncep.noaa.gov/products/analysis_monitoring/enso_advisory/ensodisc.shtml).

However, Varotsos et al. [19] showed that the 2015–2016 El Niño would be rather "moderate to strong" and not "one of the strongest on record", as that of 1997–1998, by applying the new analysis described in detail in [20] on the SOI time series for the period 1876–2015. That analysis employed a non-linear dynamics tool for detecting precursory signals of the strong El Niño events. The 2015–2016 El Niño event was "moderate to strong" and not "one of the strongest events on record."

In this paper, we focus on the already ongoing 2023-2024 El Niño event, which according to models forecasting is expected to be a strong event during the Northern Hemisphere winter (December 2023 - February 2024) (e.g., [21]. We attempt to improve the accuracy of predictions made by employing two new algorithms. The first algorithm allows the detection of precursory signals of the ENSO phase by applying to the SOI time series the recent analysis developed by Varotsos et al. [20], which has been successfully used to nowcast (i.e., short-range forecasting) the past three strong ENSO events. The second one is a recently developed nowcasting method that is applied to ONI and SOI.

 doi:10.20944/preprints202402.0202.v1

2. Materials and Methods

For our research, we use average monthly SOI values over the period January 1876 - July 2023, obtained from the Long Paddock website entitled Monthly SOI Phase 1887–1989 Base (https://data.longpaddock.qld.gov.au/SeasonalClimateOutlook/SouthernOscillationIndex/SOIDataFiles/MonthlySOIPhase1887-1989Base.txt). The SOI dataset, used in this analysis, is calculated using Troup's formula [13,14], i.e.:

$$\text{SOI} = 10\times[PA(\text{Tahiti})-PA(\text{Darwin})]/\text{SDD} \quad (1)$$

where PA represents the pressure anomaly. As mentioned above the SOI is defined as the deviation of the monthly mean sea level air pressure (i.e., P (Tahiti) − P (Darwin)) from the long-term average of P (Tahiti) − P (Darwin) for the calendar month (based on the period 1887–1989). SDD represents the standard deviation of the difference P (Tahiti) − P (Darwin) for the same calendar month (1887–1989 base period). It is useful to note that Troup's monthly SOI from 1876 onwards is derived from normalized Tahiti minus Darwin's mean sea level pressure.

In addition, in this study we use monthly mean values of ONI anomalies from January 1950 to April 2023, obtained from NOAA (https://www.cpc.ncep.noaa.gov/data/indices/oni.ascii.txt).

3. Results and Discussion

3.1. Experience Gained from Forecasting Previous Major El Niño Events as a Guide for Forecasting the 2023-2024 El Niño Using the 'Natural Time Analysis"

Our first objective is to study the evolution of the current 2023-2024 El Niño based on the conclusions drawn from the forecast analysis proposed by Varotsos et al. [19] regarding the 2015–2016 El Niño. In this context, we apply the method developed in [19,20] on the SOI dataset for the period from January 1876 to July 2023. All SOI values are considered as small, medium, or large SOI events.

Thus, we create a new time series $E_i = (\text{SOI}_i + |\text{SOI}_{min}|)$ with $i = 1,2,\dots,N$, where SOI_i (SOI_{min}) is the i-th event (minimum value) of the original SOI dataset and N is the total number of SOI events, over the entire period (January 1876 to July 2023). We then use the technique of the "natural time analysis" (NTA), matching each event E_j with the quantity N_j denoting the order of the occurrence E_j against the total number of events within a window of k events, i.e., $N_j = j/k$, with $j = 1,2,\dots,k$. Thus, we introduce a new sequence of pairs (N_j, E_j) where $E_j > 0$, using the order of events as a measure of time instead of the conventional clock time (t) [22–26].

However, the quantity $P_j = \frac{E_j}{\sum_{j=1}^{k} E_j}$, $j = 1,2,\dots,k$, could be considered as a probability, since $P_j > 0$ and $\sum_{j=1}^{k} P_j = 1$ [22,27], so we try to calculate the entropy of SOI events in the natural time domain as follows:

$$S_k = \sum_{j=1}^{k} P_j N_j ln(N_j) - \left(\sum_{j=1}^{k} P_j N_j\right) ln\left(\sum_{i=1}^{k} P_i N_i\right) \quad (2)$$

The entropy S_k is calculated for a sliding window of k-length, each time by 1 month, running the entire SOI time series of the N-events. Then, we again use Eq. (2) to calculate the entropy, but, this time, considering the time reversal in each window, i.e. $P'_j = P_{k-j+1}$, with $j = 1,2,\dots,k$, (see [19,20,23]). According to [23] the obtained entropy (S'_k) is different from S_k and the quantity $\Delta S_k = S_k - S'_k$ indicates the time symmetry breaking.

Positive values of ΔS_k correspond to a decreasing time series in natural time and when ΔS_k exceeds a certain threshold, extremely small SOI events occur, revealing El Niño (see details in [24–27]).

Furthermore, Varotsos et al. [19,20] suggested that the most useful window size for the above-described analysis is $k = 20$ events (months). Thus, we herewith calculate ΔS_{20} for the past 20 months and this window is sliding, each time by 1 month, and ran the entire SOI time series of N-events.

We also use the well-known Receiver Operating Characteristics (ROC, see [28]) method to estimate the most appropriate threshold (for ΔS_{20}) that could be used as a forecasting tool for small

 doi:10.20944/preprints202402.0202.v1

SOI events. More specifically, when $\Delta S_{k=20}$ is equal to or exceeds a certain threshold (ΔS_{thresh}) during the *i*-th month of the total period under study, an event low SOI_{i+1} (less than or equal to a specific value *T*) is predicted for the next month. If this is verified, then we have a "true positive prediction". Conversely in case $\Delta S_{20} < \Delta S_{thresh}$ and $\mathrm{SOI}_{i+1} > T$, then we have a "true negative prediction", while all other combinations lead to errors (see details in [19].

Following the classification of the past El Niño events given by the BOM (http://www.bom.gov.au/climate/enso/enlist/) we now consider a T value of -14 (see Figure 1 in [19]). We herewith present in Figure 2 the true positive rate (TPR, i.e., the number of true positive predictions in all cases with $\mathrm{SOI}_{i+1} \leq T = -14$) versus the False Positive rate (FPR, i.e., the number of false positive predictions for all cases with $\mathrm{SOI}_{i+1} > -14$) for various ΔS_{thresh}-values.

It is worth noting that the best possible prediction method yields a point in the upper left corner or coordinate (0,1) of the ROC space, representing 100% sensitivity (no false negatives) and 100% specificity (no false positives). Points along the diagonal line y = x indicate a random guess (which for a finite number of trials ranges around this diagonal (see, e.g.,[29]) while points above the diagonal indicate good prediction results (better than random) and points below the diagonal indicate poor results (worse than random).

The obtained ROC curve (for the studied period January 1876 to July 2023) best fits a function of the form $f(x) = a_1 + a_2\sqrt{x} + a_3 x^d$. So, we find that the point x_0 of the f-curve with the maximum distance $d(x)$ from the diagonal line $y = x$ (i.e., $d(x) = \frac{|x-(a_1 + a_2\sqrt{x}+a_3 x^d)|}{\sqrt{2}}$) is associated with ΔS_{thresh} = 0.0035. This value is exactly equal to the ΔS_{thresh}-value suggested by Varotsos et al [19] (for their studied period January 1878-October 2015). We note that the slope of the tangent line through the point x_0 of the f-curve (i.e., the derivative $f'(x_0)$) is unity (Figure 2).

In Figure 3, we now plot the time progression of monthly SOI events as well as the entropy change ΔS_{20} in natural time under time reversal, during the period January 2010 - July 2023. In order to further determine whether 2015–2016 El Niño could be classified as "very strong" or even more "one of the strongest on record", we again use the classification of past El Niño events provided by the BOM (http://www.bom.gov.au/climate/history/enso/).

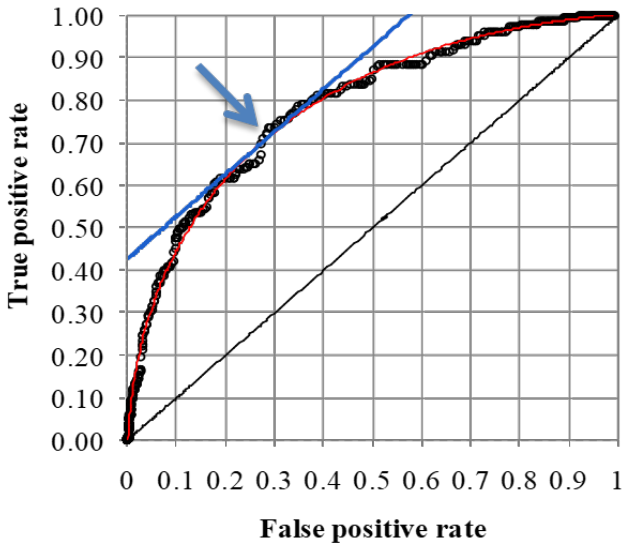

Figure 2. TPR vs. FPR (black circles) using ΔS_{20} as a predictor for the SOI event of the next month, during the period January 1876 to July 2023. The blue arrow indicates the point of the f-curve (red line) with the maximum distance of the diagonal line y = x. The slope of the tangent line (blue line) through that point of the f-curve is unity.

Preprints.org (www.preprints.org) | NOT PEER-REVIEWED | Posted: 5 February 2024 doi:10.20944/preprints202402.0202.v1

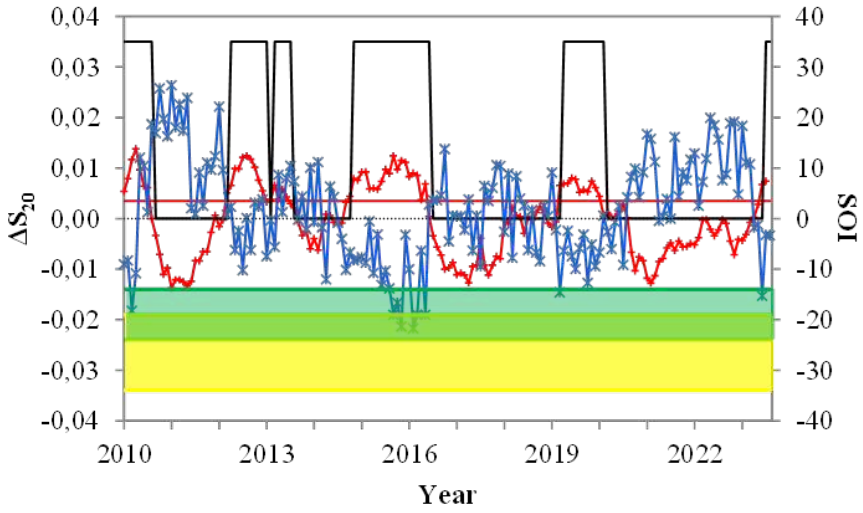

Figure 3. Monthly SOI events (blue line, right scale) as a function of time as well as the change of entropy ΔS_{20} in natural time under time reversal (red line, left scale), in the period January 2010 - July 2023. The average minimum negative SOI values together with the 1σ standard deviation bands for the two cases of "weak, weak to moderate, moderate, moderate to strong" (green band) and "strong, very strong" (yellow band) El Niño events, expressed in coloured areas. The black line represents the alarm triggered when ΔS_{20} exceeds the threshold value ΔS_{thresh} = 0.0035 (red straight line). Note: SOI values are shifted by 1 month so that a direct comparison can be made easily.

In Figure 3 the coloured areas represent the mean minimum negative SOI value together with the 1σ standard deviation bands for the two cases of "weak, weak to moderate, moderate, moderate to strong" (green band) and "strong, very strong" (yellow band) El Niño events. We notice in Figure 3 that the monthly SOI events, for the period 2015–2016, remain in the green zone and on the yellow border.

Furthermore, looking at Figure 1 in Varotsos et al. [19], it appears that the SOI time series during the period 2015–2017 presents a less pronounced downward trend compared to the corresponding ones during El Niño events of previous periods such as 1982–1983 and 1997–1998 (see Figure 4).

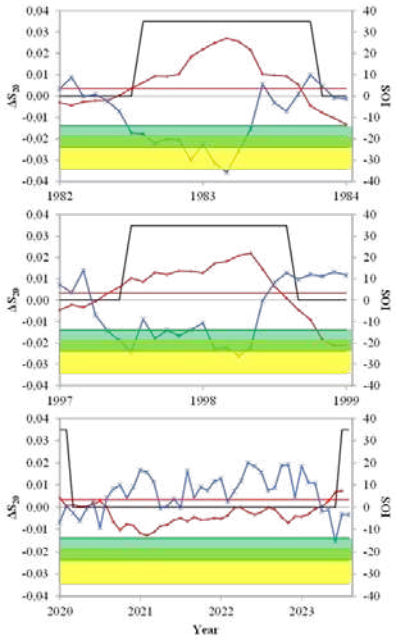

 doi:10.20944/preprints202402.0202.v1

Figure 4. As in Figure 3, but only for the 1982–1983, 1997–1998 (the two strongest of the last century), and the ongoing 2023–2024 El Niño events.

These observations lead to the conclusion that the forecasting analysis proposed by Varotsos et al. [19], is fully validated, and the 2015-2016 El Niño was rather characterized as a "moderate to strong" event rather than "one of the strongest on record".

3.2. On the Progress of the 2023–2024 El Niño Event Using the 'Natural Time Analysis"

Based on our above-described experience from the forecasting of the earlier major El Niño events we proceed to our second objective to further investigate claims for a very strong 2023-2024 El Niño. However, as clearly shown in Figure 4, the monthly SOI events, during January 2021–May 2023, remain above the green zone, after an increasing trend, and an abrupt decline occurs in June 2023 without foreshadowing a strong El Niño. Moreover, the variation of ΔS_{20} during the 2023-2024 El Niño in comparison with 1982–1983 and 1997–1998 El Niño events is not as sharp, and an alarm (i.e., $\Delta S_{20} \geq \Delta S_{thresh}$) is detected only in May and June 2023.

To estimate the extent of ΔS_{20} variation (associated with SOI variation), we plot in Figure 5 the histogram of ΔS_{20} and the probability density function (PDF) obtained by the estimator:

$$f_N(\Delta S_{20}) = \frac{1}{NB_N}\sum_{i=1}^{N} K\left(\frac{\Delta S_{20} - T_i}{B_N}\right) \quad (3)$$

In equation (3) T_i are the observed values of ΔS_{20} during the period January 1880-July 2023, N is the total number of these observations, the kernel $K(x) = \begin{cases} \frac{3(1-x^2)}{4}, & |x| < 1 \\ 0, & |x| \geq 1 \end{cases}$ and $B_N = 10.25\,\frac{\sigma}{N^{0.34}}$ with σ the standard deviation of the observed ΔS_{20} values (Mercik et al., 1999).

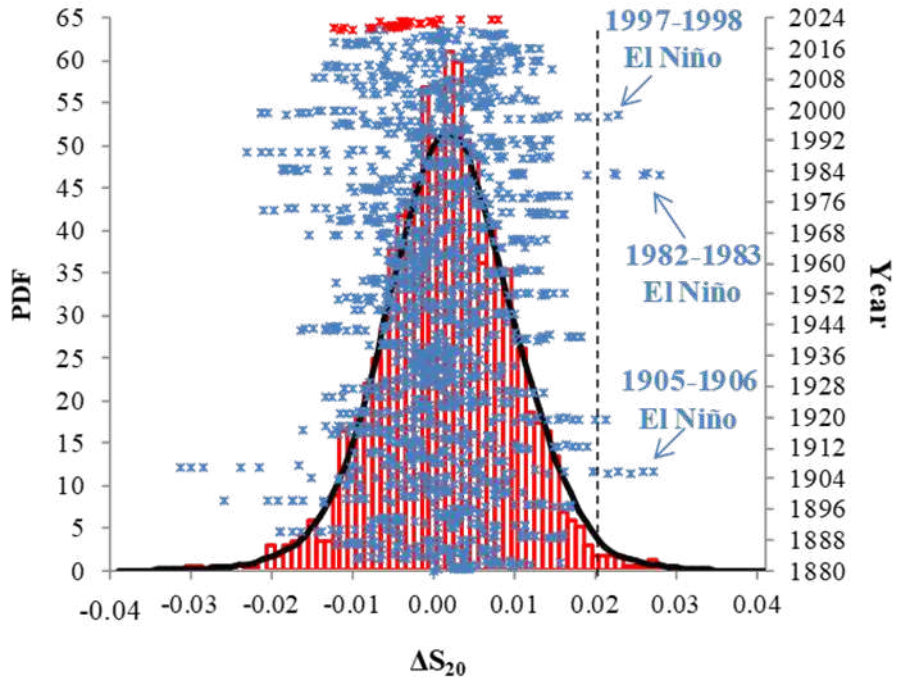

Figure 5. The PDF of ΔS_{20} (black curve, left scale) with the corresponding histogram (red bars, left scale) obtained from the ΔS_{20} time series from January 1880-July 2023, which is also plotted against time (blue points, right scale) along the vertical axis. Blue arrows indicate the ΔS_{20}-values that exceed the 99%-percentile, $p_{99\%} = 0.02$ of the total dataset ($p_{99\%}$ is depicted with the vertical dashed black line). These extremes are characterized by correspondingly strong El Niño events. The red points and label show the ΔS_{20}-values during January 2021 – July 2023.

 doi:10.20944/preprints202402.0202.v1

3.3. Forecasting El Niño Events Using the "Modified Natural Time Analysis" Applied to ONI

We now investigate the distribution of ONI values, labelled by x, over the period from January 1950 to April 2023, using the Modified Natural Time Analysis (M-NTA). By applying the non-parametric Kolmogorov Smirnov (KS) test, we test the hypothesis H_o: the sample values follow a normal distribution against H_1: the sample values do not follow the normal distribution (Figure 6a). The calculated KS-statistic Dn and the corresponding p-values are 0.043 and 0.076, respectively. From $0.076 > 0.05$ we conclude that the dataset fits the normal distribution well, at the 95% confidence level.

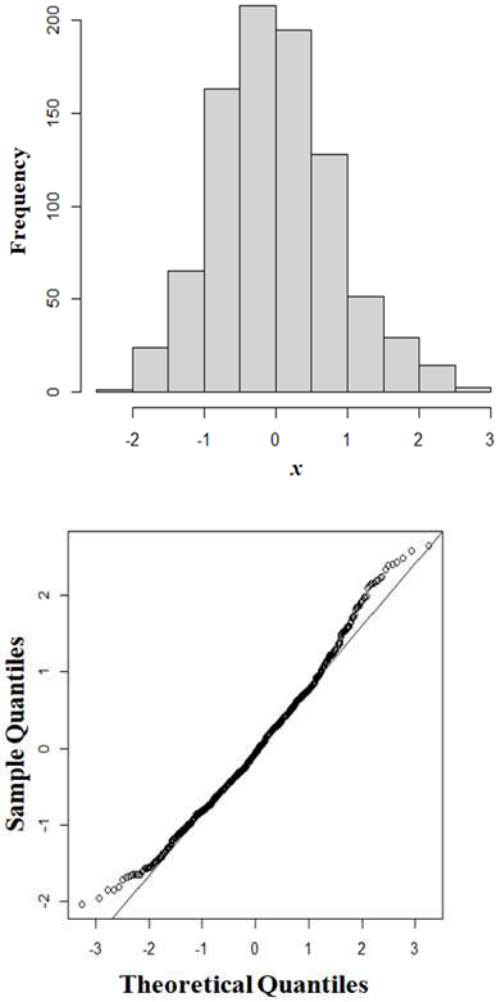

Figure 6. (a) Histogram for the monthly mean x values of the ONI dataset over the period January 1950 – April 2023 obtained from NOAA. (b) Normal Q-Q plot for the studied ONI values.

However, this is inconsistent with the quantile-quantile (Q-Q) plot shown in Figure 6b, which is a graphical method for assessing whether two data sets come from populations with a common distribution. The vertical axis depicts the sample quantiles, while the horizontal axis represents the theoretical quantiles. According to Figure 6b, the ONI values seem to diverge from the normal distribution, and the inconsistency is mainly attributed to the extreme values of the data set. To clarify this point, we apply a newly developed nowcasting method, suggested by Varotsos et al. [30–32]. This method is a modified NTA (M-NTA) and its steps are described below:

We plot the logarithm of the cumulative number (C_N) of the ONI observations equal to or above a certain x-value versus the x magnitude (Figure 7). For high ONI values, regression analysis shows a statistically significant linear fit between $\log C_N$ and x. The best linear fit is achieved for the range (−0.11, 1.93):

Preprints.org (www.preprints.org) | NOT PEER-REVIEWED | Posted: 5 February 2024 doi:10.20944/preprints202402.0202.v1

$$C_N' = 10^{a_1} \cdot \left(10^{a_0 x} - 10^{a_0 x_{max}}\right) \quad (4)$$

The F-test (t-test) suggests that the calculated values of R^2 = 0.99 (a_0 = −0.69 and a_1 = 2.67) are statistically significant (at 95% confidence level) thus giving indications that high ONI values may follow a semi-logarithmic distribution resembling the Gutenberg-Richter (GR) law (Varotsos et al. 2020b, 2004, 2021).

To fit ONI values above rollover (i.e., $x \geq 1.93$), we use an upper-truncated GR model developed by Burroughs and Tebbens (2002):

$$C_N' = 10^{a_1} \cdot \left(10^{a_0 x} - 10^{a_0 x_{max}}\right) \quad (5)$$

where the values a_0, a_1 are derived from Eq. (4) and x_{max} = 2.72 is chosen to obtain the most accurate approximation.

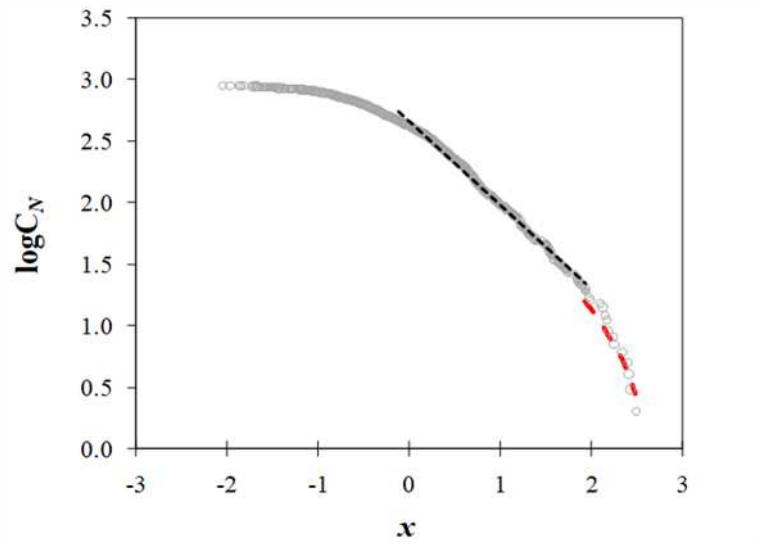

Figure 7. Semi-log plot of cumulative number (C_N) of ONI values greater than or equal to x vs x (gray circles). The dashed black line is the least-squares fit of the GR-scaling ($\log C_N = 2.66 - 0.69 \cdot x$ with R^2 = 0.99), while the dashed red line is the upper-truncated fit derived from Eq. (5) with x_{max} = 2.72.

Next, we use the NTA in order to study the exceptional events in a time series. As we said above "natural time" ignores the clock-time that an event occurs and instead provides an index that is the order of occurrence of that event divided by the total number of events in the time-series [24,26,33,34]. In this sense, we detect the high ONI values (with $x \geq x_2$) in the studied time series, and every time a high ONI value occurs, we calculate the cumulative numbers C_{N1}, C_{N2} of the ONI values with magnitude $x \geq x_1$, $x \geq x_2$ respectively (where $x_1 < x_2$) that occur after this high ONI value until the end of the time series. The x_1 value is chosen as the average of the ONI dataset (i.e.−0.003), while the value x_2 = 0.826 is set and corresponded to the mean increased by the standard deviation of the dataset.

The above-mentioned technique allows us to precisely test the accuracy of the GR fit by examining whether two values with constant difference $x_2 - x_1$ have a constant ratio: $\frac{C_{N2}}{C_{N1}}$ as predicted by the GR relation:

$$\frac{C_{N2}}{C_{N1}} = 10^{a_0 \cdot (x_2 - x_1)} = \text{constant} \quad (6)$$

where a_0 is estimated from Eq. (4) and C_{N1}, C_{N2} is the cumulative number of ONI values with magnitude $x \geq x_1$, $x \geq x_2$ respectively.

Preprints.org (www.preprints.org) | NOT PEER-REVIEWED | Posted: 5 February 2024 doi:10.20944/preprints202402.0202.v1

Indeed, we plot the pairs (C_{N1}, C_{N2}) in Figure 8a, and an almost perfect linear fit $f(C_{N1}) = A \cdot C_{N1}$ (with $A = 0.27$ and $R^2 = 0.97$), thus confirming the accuracy of the GR- fit.

The NTA is also used to forecast the occurrence rate of future extreme ONI events, based on the estimated mean occurrence rate of the lowest (and most frequent) ONI values.

To this end, we first plot C_{N1} versus the clock time t (during January 1950 – April 2023) where a nearly perfect linear fit $h(t) = b \cdot t$ on the pairs (C_{N1}, t) emerges (Figure 8b). The constant $b = 0.45 \pm 0.04$ is estimated by the average of the ratio $\frac{C_{N1}}{t}$ and its confidence interval is:

$$\left(b - Z_{a/2}\sqrt{\frac{b(1-b)}{n}}, b + Z_{a/2}\sqrt{\frac{b(1-b)}{n}} \right)$$

where n is the count of the pairs (C_{N1}, t) and $Z_{a/2}$ is the critical value of the standard normal distribution at a significance level.

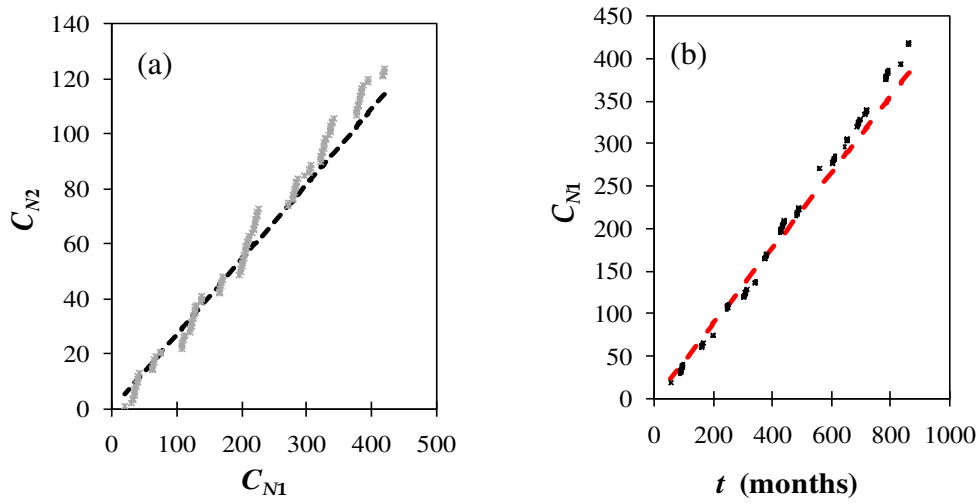

Figure 8. (*a*) Dependence of cumulative number C_{N2} of high ONI values with magnitude $x \geq x_2$ on the cumulative number C_{N1} of ONI values with $x \geq x_1$ (grey points). The dashed black line is the linear fit on the pairs (C_{N1}, C_{N2}) with $f(C_{N1}) = AC_{N1}$, where $A = 0.27$ and $R^2 = 0.97$. (*b*) Cumulative number C_{N1} of ONI values with $x \geq x_1$ vs. clock time [in months], over the period January 1950 – April 2023 (black dots). The red dashed line is the linear fit on the pairs (C_{N1}, t) with $h(t) = bt$, where $b = 0.45$ and $R^2 = 0.98$.

The extracted $R^2 = 0.98$ indicates high statistical significance at the 95% confidence level. Then, utilizing all the above, we attempt to predict the occurrence rate $\frac{C_N{}'}{t}$ and consequently the average time interval between two successive ONI values with $x \geq x_0$ for some selected high magnitudes i.e., $1.74 \leq x_0 \leq 2.64$, using the following formula which derives from Eq. (6):

$$\frac{C_N{}'}{t} = 10^{a_0 \cdot (x_0 - x_1)} \cdot b \qquad (7)$$

where b is seen in Figure 8b (Table 1).

 doi:10.20944/preprints202402.0202.v1

Table 1. The nowcasted mean inter-event time t [in years] for ONI values with magnitude $1.74 \le x_0 \le 2.48$ accompanied by the lower and upper limit of the 95%-confidence interval of t. The numbers in black (gray) color derive from the ONI time series with real (reversed) time evolution.

ONI value x_0	Nowcasted mean inter-event time t [in years]	The lower limit of the 95%-confidence interval of t.	The upper limit of the 95%-confidence interval of t.
1.74	3.0 *(2.6)*	2.5 *(2.2)*	3.7 *(3.2)*
1.84	3.5 *(3.1)*	2.9 *(2.6)*	4.3 *(3.8)*
1.94	4.1 *(3.6)*	3.4 *(3.1)*	5.1 *(4.4)*
2.04	4.8 *(4.3)*	4.0 *(3.6)*	6.0 *(5.2)*
2.14	9.2 *(8.2)*	7.6 *(6.9)*	11.4 *(10.0)*
2.24	12.1 *(10.8)*	10.1 *(9.2)*	15.1 *(13.2)*
2.57	51.4 *(45.9)*	42.8 *(38.9)*	64.3 *(56.0)*
2.64	102.1 *(91.2)*	85.1 *(77.3)*	127.6 *(111.1)*

It is worth noting that, in case of extremely high ONI values (with $x \ge 1.93$) we use the truncated GR scaling given in Eq. (5) (i.e., $\frac{C_N'}{t} = \frac{10^{a_0 \cdot x_0} - 10^{a_0 \cdot x_{\max}}}{10^{a_0 \cdot x_1} - 10^{a_0 \cdot x_{\max}}} \cdot b$).

The last step of our survey is to repeat the NTA, this time, applied to a new time series, which is generated by the initial ONI time series having reversed its time evolution. The analysis gives similar results (i.e., $f(C_{N1}) = 0.27 C_{N1}$ with $R^2 = 0.99$ and $b = 0.50 \pm 0.04$ with $R^2 = 0.995$), and the estimated nowcasted mean inter-event time for the selected ONI values are presented in Table 1 (with grey colour).

According to Thompson [13] the phenomenon "El Niño" has arrived causing major changes to the weather all over the world. This year or next is going to be the hottest year on record, as happened in 2016. She also suggests that the 2016 El Niño was comparable in strength to the one in 1998 (see also [16]. The ONI values from October 1997 to January 1998 (i.e., 2.33, 2.4, 2.39, 2.24, respectively), as well as the ONI value from October 2015 to January 2016 (i.e., 2.42, 2.57, 2.64, 2.48, respectively), are seen to be the maxima of the total time-series (see Figure 9).

Using the M-NTA the estimation of the mean inter-event time for the ONI value occurred in November 1997 (i.e., $x_0 = 2.4$) is between 17.4 years and 26.1 years, a forecasting that sufficiently describes the empirical inter-event time from 1997 to 2016 (see Table 1). Furthermore, in December 1982 (i.e., 15 years before December 1997) the ONI value is $x_0 = 2.23$ which corresponds to the estimated inter-event time (9.8, 14.7) years, revealing a good agreement between the nowcasted and the empirical time. Finally, using Table 1 we can predict that the mean time for the re-appearance of the ONI values observed in November 2015 and December 2015, i.e., 2.57 and 2.64 is expected to be (42.8, 64.3) years and (85.1, 127.6) years respectively.

 doi:10.20944/preprints202402.0202.v1

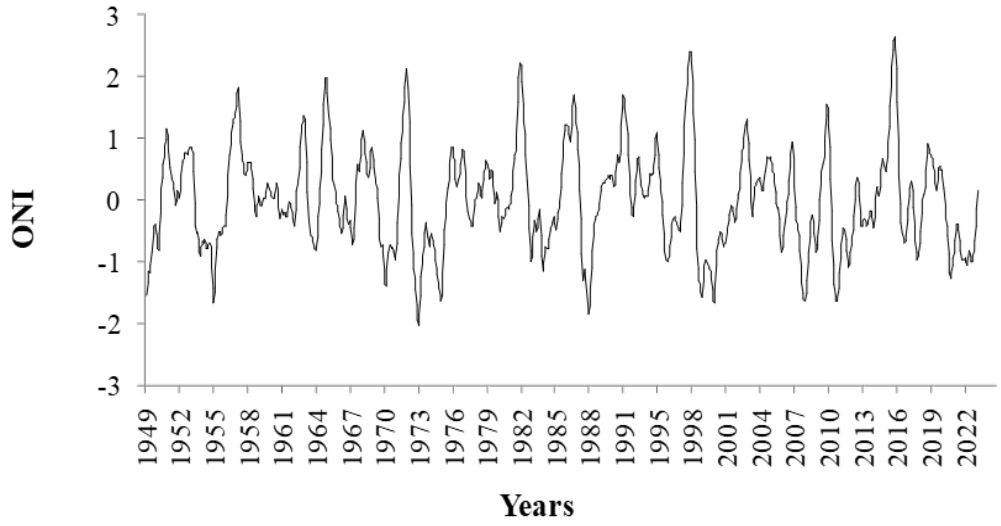

Figure 9. Monthly mean ONI (ºC) values over the period January 1950 – April 2023 (obtained from NOAA).

Regarding the prediction of the new El Nino event, this is linked to the extreme values of many previous years. For example, in November 1997 we had an extreme ONI-value = 2.40 which according to the model is expected to reappear in (17.4, 26.1) years, possibly reaching 2023. On the other hand, from October 2015 to December 2015 extreme ONI values i.e., 2.42, 2.57, 2.64 arose which according to the model may be repeated in [18.9, 28.3] years, (42.8, 64.3) years and (85.1, 127.6) years, respectively. Therefore, extreme value is difficult to reappear in 2023 (originating from 2015-2016 with ONI-value ≥ 2.42) but can appear originating from 1997 (with ONI-value ≈ 2.40).

However, it is very likely that for the winter of 2023-2024, a large ONI-value associated with 2015-2016 will appear since in September 2015 and February 2016 we had a large ONI-value = 2.16 and ONI-value = 2.14 respectively, which according with the model they will repeat in (8.0, 12.0) years and (7.6, 11.4) years, possibly reaching 2023-2024.

3.4. Forecasting El Niño Events Using the "Modified Natural Time Analysis" Applied to SOI

To confirm the above-mentioned results, we apply the same M-NTA method on the SOI dataset during the period January 1950-April 2023, focusing on the low SOI-values that appear to dominate during the three strong ENSO events (1982–1983, 1997–1998, 2015-2016).

Thus, we plot the logarithm of the cumulative number (c_N) of the SOI observations equal to or below a certain x-value against x. For low SOI values, the regression analysis gives a statistically significant linear fit between $\log c_N$ and x (i.e., $\log c_N = a_3 + a_2 x$) with optimal features in the range of values (-∞, -3.1] where the calculated values of $R^2 = 0.99$ ($a_2 = 0.07$ and $a_3 = 2.86$) are statistically significant (at 95% confidence level).

Then, we detect the low SOI values (with $x \le x_2$) in the studied time series, and every time a low SOI value occurs, we calculate the cumulative numbers c_{N1}, c_{N2} of the SOI values with magnitude $x \le x_1$, $x \le x_2$ respectively (where $x_1 < x_2$) that occur after this low SOI value until the end of the time series. The x_1 value is chosen as the threshold of the above-mentioned value range (-∞, -3.1], while the value $x_2 = -8.2$ is the 20% percentile of the entire dataset.

Plotting the pairs (c_{N1}, c_{N2}), a perfect linear fit $f(c_{N1}) = A \cdot c_{N1}$ (with $A = 0.44$ and $R^2 = 0.99$) confirms the accuracy of the GR- fit. We then plot c_{N1} against clock time t (during January 1950 – April 2023) and a statistically significant (at 95% confidence level) linear fit $h(t) = b \cdot t$ (with $b = 0.36 \pm 0.04$ and $R^2 = 0.98$) is revealed.

Finally, using the above results, we forecast the occurrence rate $\frac{C_N'}{t} = 10^{a_0 \cdot (x_0 - x_1)} \cdot b$ and consequently the average time interval between two successive SOI values with $x \le x_0$. In this regard,

 doi:10.20944/preprints202402.0202.v1

we select the low SOI values with -35.7 ≤ x_0 ≤ -19.0, i.e., values like those observed during the three strong ENSO events (Table 2).

Using Table 2, we see that the average time for the SOI values observed in October 2015 and January 2016 (i.e., -21.30 and -21.7) to reappear is (4.5, 6.8) years and (4.9, 7.2) years respectively, while the SOI magnitudes in November 1982 and March 1998 (i.e., -30 and -26.1) correspond to (20.6, 30.6) years and (10.4, 15.6) years, respectively.

Table 2. The nowcasted mean inter-event time t [in years] for SOI values with magnitude x_0 from -35.7 to -19.0 accompanied by the lower and upper limit of the 95%-confidence interval of t.

SOI value x_0	Nowcasted mean inter-event time t [in years]	The lower limit of the 95%-confidence interval of t	The upper limit of the 95%-confidence interval of t
-19.0	3.6	3.0	4.5
-21.3	5.4	4.5	6.8
-21.7	5.8	4.9	7.2
-26.1	12.5	10.4	15.6
-30.0	24.6	20.6	30.6
-31.4	31.4	26.2	39.1
-35.7	66.3	55.4	82.5

However, all these extremely low values seem to not affect the current ENSO event (2023-2024). On the other hand, the January 1983 SOI value (i.e., -31.4) corresponds to (26.2, 39.1) years and it could be related to the 2015-2016 ENSO, while the February 1983 SOI value (i.e., -35.7) corresponds to (55.4, 82.5) years and is expected to affect the years after 2038. As for the SOI value of May 2023 (i.e., -15.26), it may be related to the minimum SOI of 2019 (i.e., -14.6).

4. Conclusions

Applying NTA and M-NTA to SOI and ONI data we explored the forecasting ability and accuracy of the three strong ENSO events (1982–1983, 1997–1998, 2015-2016) to derive the characteristics of the ongoing 2023-2024 El-Niño event. The main findings that emerged are obtained are the following:

1) Forecasting analysis performed by both NTA and M-NTA verified that the 2015-2016 El Niño was characterized as a “moderate to strong” event and not “one of the strongest on record”, as various forecasting reports of that period claimed.
2) The SOI time series during the period January 2021 - July 2023 shows a variance that doesn’t foreshadow a strong 2023-2024 El Niño. Furthermore, the variation of entropy change in natural time, during the 2023-2024 El Niño, is less pronounced compared to the corresponding ones during past El Niño events. Finally, according to the probability density function of the ΔS_20 dataset, all the values during January 2021-July 2023 remain below the threshold m + s, where m (s) is the mean (standard deviation) of the dataset.
3) The M-NTA model appears to adequately estimate the interevent time from 1982 to 1997, two years that correspond to exceptional ONI values of the overall time series. The estimated time of the intermediate event between 1997 and 2016 is estimated to be (17.4, 26.1) years. The average recurrence time of the ONI extremes observed in 2015 was found to be between (18.9, 127.6) years.
4) Regarding the intensity of the ongoing 2023-2024 El Nino event, an ONI value 2.64 occurred only in 2015 (moderate to strong El Nino) and the model predicts a recurrence period of over 85 years.

So, it is unlikely to reappear in 2023. Instead, values from 2.14 to 2.40 coming from 1997 or 2016 may appear.

5) The extremely low SOI values observed in the last three strong ENSO events do not appear to be related to the ongoing ENSO event (2023-2024). On the other hand, the January 1983 SOI value could be related to the 2015-2016 ENSO, while the February 1983 SOI value is expected to affect years after 2038. As for the May 2023 SOI value, it may be related to the minimum SOI of 2019.

The afore-mentioned analytical tools may be applied to paleoclimatic data to predict extreme environmental phenomena that may lead to severe ecological impacts [31].

Author Contributions: Conceptualization, C.V. and Y.M.; methodology, N.S., M.E., and C.V.; software, N.S. and M.E.; validation, C.V., N.S. and M.E.; formal analysis, M.E. and N.S.; investigation, C.V.; N.S. and M.E.; resources, Y.M. and D.S..; data curation, M.E.; supervision, C.V. All authors have read and agreed to the published version of the manuscript.

Funding: This research received no external funding.

Data Availability Statement: The data will be available upon request.

Conflicts of Interest: The authors declare no conflicts of interest.

References

1. Walker, G.T.; Bliss, E.W. World Weather V. *Mem. Roy. Meteor. Soc.* **1932**, *4* (36), 53-84.
2. Power, S.B.' Kociuba, G. The impact of global warming on the Southern Oscillation Index. *Clim. Dyn*. **2011,** *37*, 1745–1754. https://link.springer.com/article/10.1007/s00382-010-0951-7.
3. Rasmusson, E.M.; Carpenter, T. H. Variations in tropical sea surface temperature and surface wind fields associated with the Southern Oscillation/El Niño. *Mon. Weather Rev*. **1982,** *110*(5), 354-384. https://doi.org/10.1175/1520-0493(1982)110<0354:VITSST>2.0.CO;2.
4. Troup, A.J. The Southern Oscillation. *Q. J. R. Meteorol. Soc.* **1965,** *91*, 490–506. https://rmets.onlinelibrary.wiley.com/doi/abs/10.1002/qj.49709139009.
5. Yun, KS., Lee, JY., Timmermann, A. et al. Increasing ENSO–rainfall variability due to changes in future tropical temperature–rainfall relationship. *Commun. Earth Environ.* **2021,** *2*, 43. https://doi.org/10.1038/s43247-021-00108-8, 2021.
6. Neelin, J.D.; Latif, M. El Nino dynamics. *Phys. Today* **1998,** *51*(12), 32. doi: 10.1063/1.882496.
7. Cai, W.; Ng, B.; Geng, T. et al. Anthropogenic impacts on twentieth-century ENSO variability changes. *Nat. Rev. Earth Environ***. 2023**, *4*, 407–418. https://doi.org/10.1038/s43017-023-00427-8.
8. Singh, M.; Sah, S.; Singh, R. The 2023-24 El Niño event and its possible global consequences on food security with emphasis on India. *Food Sec*. **2023**, *15*, 1431–1436. https://doi.org/10.1007/s12571-023-01419-8.
9. Ubilava, D.; Abdolrahimi M. The El Niño impact on maize yields is amplified in lower income teleconnected countries. *Environ. Res. Lett.*, **2019**, *14* Article 054008. https://iopscience.iop.org/article/10.1088/1748-9326/ab0cd0/meta.
10. Glantz, M.H.; Ramirez, I.J. Reviewing the Oceanic Niño Index (ONI) to Enhance Societal Readiness for El Niño's Impacts. *Int. J. Disaster Risk. Sci*., **2020**, *11*, 394–403. https://doi.org/10.1007/s13753-020-00275-w.
11. Gurdek-Bas, R.; Benthuysen, J.A.; Harrison, H.B. et al.: The El Niño Southern Oscillation drives multidirectional inter-reef larval connectivity in the Great Barrier Reef. *Sci. Rep.* **2022**,*12*, 21290. https://doi.org/10.1038/s41598-022-25629-w
12. Khanke, H. R.; Azizi, M.; Asadipour, E.; Barati, M. Climate Changes and Vector-borne Diseases with an Emphasis on Parasitic Diseases: A Narrative Review. *Health Emerg. Disasters Quart.,* **2023** *8*(4), 293-300, http://dx.doi.org/10.32598/hdq.8.4.276.12023.
13. Thompson A. El Niño May Break a Record and Reshape Weather around the Globe. *Scientific American***, 2023**, https://www.scientificamerican.com/article/el-nino-may-break-a-record-and-reshape-weather-around-the-globe/.
14. Yin, J.; Xu, J.; Xue, Y.; Xu, B.; Zhang, C.; Li, Y.; Ren, Y. Evaluating the impacts of El Niño events on a marine bay ecosystem based on selected ecological network indicators. *Sci. Total Environ.,* **2021**, *763*, 144205, https://doi.org/10.1016/j.scitotenv.2020.144205.
15. Barber, R.T.; Chavez, F.P. Biological consequences of El Nino. *Science*. **1983**, *222*(4629), 1203-1210. https://www.science.org/doi/abs/10.1126/science.222.4629.1203.
16. WMO: **2022**, https://public.wmo.int/en/our-mandate/climate/el-ni%C3%B1ola-ni%C3%B1a-update.
17. Hamlington, B. D.; Willis, J. K.; Vinogradova, N. The emerging golden age of satellite altimetry to prepare humanity for rising seas. *Earth's Future*, **2023**, 11(11), e2023EF003673, https://doi.org/10.1029/2023EF003673.

18. Omid, A. Advances and challenges in climate modeling. *Climatic Change,* **2022**, *170*(1-2), https://doi.org/10.1007/s10584-021-03298-4.
19. Varotsos, C.A.; Tzanis, C.G.; Sarlis, N.V. On the progress of the 2015–2016 El Niño event. *Atmos. Chem. Phys*., **2016a**, *16*, 2007–2011. https://doi.org/10.5194/acp-16-2007.
20. Varotsos, C.A.; Tzanis, C.; Cracknell, A.P. Precursory signals of the major El Niño Southern Oscillation events. *Theor. Appl. Climatol.,* **2016b,** *124*(3), 903-912. https://link.springer.com/article/10.1007/s00704-015-1464-4.
21. National Oceanic and Atmospheric Administration (NOAA), El Niño/Southern Oscillation (ENSO) Diagnostic Discussion, issued by Climate Prediction Center. **2023**, https://www.cpc.ncep.noaa.gov/products/analysis_monitoring/enso_advisory/ensodisc.shtml.
22. Varotsos, P. A.; Sarlis, N.V.; Skordas, E.S. Long-range correlations in the electric signals that precede rupture. *Phys. Rev. E,* **2002**, *66*, 011902. https://journals.aps.org/pre/abstract/10.1103/PhysRevE.66.011902.
23. Varotsos, P. A.; Sarlis, N.V.; Tanaka, H.K.; Skordas, E.S. Some properties of the entropy in the natural time. *Phys. Rev. E*, **2005**, *71*, 032102. https://doi.org/10.1103/PhysRevE.71.032102.
24. Sarlis, N.V.; Skordas, E.S.; Varotsos, P.A. Nonextensivity and natural time: The case of seismicity. *Phys. Rev. E,* **2010** *82*, 021110. https://journals.aps.org/pre/abstract/10.1103/PhysRevE.82.021110..
25. Sarlis, N.V.; Skordas, E.S.; Varotsos, P.A. Similarity of fluctuations in systems exhibiting Self-Organized Criticality, *EPL* **2011a** ,*96*, 28006. https://doi.org/10.1209/0295-5075/96/28006,.
26. Sarlis, N.V.; Skordas, E.S.; Varotsos, P.A. The change of the entropy in natural time under time-reversal in the Olami– Feder–Christensen earthquake model. *Tectonophysics,* **2011b**, *513,* 49– 53. https://doi.org/10.1016/j.tecto.2011.09.025.
27. Varotsos, P.A.; Sarlis, N.V.; Skordas, E.S. Natural Time Analysis: The new view of time. Precursory Seismic Electric Signals, Earthquakes and other Complex Time-Series. Springer-Verlag, Berlin Heidelberg. ISBN 978-3-642-16449-4, DOI 10.1007/978-3-642-16449-1, **2011**.
28. Fawcett, T. An introduction to ROC analysis. *Pattern Recogn. Lett.,* **2006**, *27*, 861–874. https://doi.org/10.1016/j.patrec.2005.10.010.
29. Sarlis, N.V.; Christopoulos, S.-R.G. Visualization of the significance of Receiver Operating Characteristics based on confidence ellipses. *Comput. Phys. Commun*.**,** **2014** *185*, 1172–1176. http://dx.doi.org/10.1016/j.cpc.2013.12.009.
30. Varotsos, C.A.; Efstathiou, M.N.; Christodoulakis, J. The lesson learned from the unprecedented ozone hole in the Arctic in 2020 A novel nowcasting tool for such extreme event. *J. Atmos. Sol.-Terr. Phys*., **2020a,** *207*, 105330. https://doi.org/10.1016/j.jastp.2020.105330.
31. Varotsos C.A.; Mazei Y.; Novenko E.; Tsyganov A.N.; Olchev A.; Pampura T.; Mazei N.; Fatynina Y.; Saldaev D.; Efstathiou M.A. New Climate Nowcasting Tool Based on Paleoclimatic Data. *Sustainability*, **2020b,** *12*, 5546. https://doi.org/10.3390/su12145546.
32. Varotsos, C.A.; Mazei, Y.; Saldaev, D.; Novenko, E.; Efstathiou, M.; Voronova, T.; Xue, Y. Nowcasting of air pollution episodes in megacities: A case study for Athens, Greece. *Atmos. Pollut. Res.,* **2021**, *12*, 101099. https://doi.org/10.1016/j.apr.2021.101099.
33. Varotsos P.A.; Sarlis N.V.; Skordas E.S. Order parameter fluctuations in natural time and b-value variation before large earthquakes. *Nat. Hazards Earth Syst. Sci*., **2012**, *12*(11), 3473-3481. https://doi.org/10.5194/nhess-12-3473-2012.
34. Varotsos P.A.; Sarlis N.V.; Skordas E.S.; Tanaka H. A plausible explanation of the b-value in the Gutenberg-Richter law from first Principles. *Proc. Jpn. Acad., Ser. B*, **2004**,*80*(9), 429-434. https://www.jstage.jst.go.jp/article/pjab/80/9/80_9_429/_article/-char/ja/.